ANNUALLY-RESOLVED SEDIMENTATION OF THE MIDDLE MIOCENE CLARKIA LAKE DEPOSIT (USA)

A Thesis

by

DAIANNE FRANCIS HOFIG

Submitted to the Office of Graduate and Professional Studies of
Texas A&M University
in partial fulfillment of the requirements for the degree of

MASTER OF SCIENCE

Chair of Committee, Yi Ge Zhang
Committee Members, Ethan Grossman
Franco Marcantonio
Jason West
Head of Department, Shari Yvon-Lewis

May 2021

Major Subject: Oceanography

ABSTRACT

Lacustrine varved sediments are high-resolution paleoenvironmental archives, in which their layers function as temporal markers of seasonality. The temporal framework of such records is required to improve benchmark climate models because they offer snapshots of past climate systems within annual to millennial timescales. The middle Miocene Clarkia Lake Deposit (Idado, USA) is a plant fossil *Lagerstätte* containing varve-like sediments deposited during the Miocene Climate Optimum, a phase of global warming and carbon cycle perturbation at ca. 16 million years ago. Despite being extensively studied in the past decades, its absolute age and temporal relationship with the Columbia River Flood Basalt, and the causes of the varves remained elusive. This study presents the first tephra-derived U-Pb zircon ages for the Clarkia Lake Deposit and an age model based on spectral analysis of elemental and color distribution of the sediments obtained via micro X-Ray fluorescence. The results show that the Clarkia Lake Deposit (1) is dated at 15.78 ± 0.03 Ma, after the most intense eruption phases of the Columbia River Flood Basalt Group; and (2) represents ~840 varve-years. These stratigraphic relationships highlight the Clarkia Lake Deposit as a high-resolution archive of the Miocene Climate Optimum, in a greenhouse world that may be employed as an analog for modeling future Earth's climate.

DEDICATION

To Antonio, Silvéria, Hellen, and Kaio.

ACKNOWLEDGEMENTS

I want to thank my committee chair and advisor, Yi Ge Zhang, for offering me an opportunity to work on such a fascinating project, in which I grew as a scientist because I felt welcomed as a valuable team member of his group. His thorough scientific questioning and big-picture focus always inspired me to try harder and reach higher every day. I owe him my endless gratitude for supporting me in the most difficult patches of my journey inside and outside graduate school. I found the same compassion and guidance in my committee members, Ethan Grossman, Franco Marcantonio, and Jason West. I will always keep their advice as important lessons for my future career. I am thankful to Hong Yang and Qin Leng from Bryant University, who are not only incredible collaborators and admirable scientists but friends I hold dear in my heart.

I am grateful for the supportive community of friends, colleagues, department faculty, and staff of the Department of Oceanography at Texas A&M University. The bright intellect of my labmates is only eclipsed by their endless kindness and friendship. Noura, Xiaoqing, Ronnie, and Bumsoo: thank you so much! I am so lucky for having Jess Fitzsimmons in my life; she embodies the type of person and researcher I want to become one day. I am beyond words to thank Chrissy Wiederwohl for her support and advice throughout this journey.

Finally, thanks to my family for their encouragement and unwavering support. This work would not be possible without your infinite patience and love.

CONTRIBUTORS AND FUNDING SOURCES

Contributors

This work was supervised by a thesis committee consisting of Dr. Yi Ge Zhang of the Department of Oceanography, Prof. Ethan Grossman and Prof. Franco Marcantonio of the Department of Geology, and Dr. Jason West of the Department of Ecosystem Science and Management.

Part of the U-Pb zircon data measurements for this thesis was provided by Prof. Brent Miller, Prof. Hong Yang, and Prof. Qin Leng. Micro X-ray fluorescence data were acquired in collaboration with Dr. Liviu Giosan.

All other work conducted for the thesis was completed by the student independently.

Funding Sources

Graduate study was supported by the A.T. Webber, James Sharp, Donald & Melba Ross scholarships from the College of Geosciences, Department of Oceanography as well as Lechner Graduate Scholarship from the Texas A&M University.

This work was made possible by National Science Foundation (NSF) under Grant Number EAR-1806015. Its contents are solely the responsibility of the authors and do not necessarily represent the official views of the Texas A&M University and NSF.

TABLE OF CONTENTS

Page

LIST OF FIGURES

Page

1. INTRODUCTION

The interplay between the augmented anthropogenic carbon dioxide (CO_2) emissions into the atmosphere since the dawn of the industrial revolution in 1750 and the significant global surface warming has been the locus of climate research efforts since the late 1970s (e.g., Charney *et al.*, 1979). Despite substantial progress in the last four decades in shedding light on the role of greenhouse gases in biogeochemical cycles (Stocker *et al.*, 2013), climate models addressing future scenarios are bound by uncertainty due to the unprecedented carbon release rates to the atmosphere (Zeebe, Ridgwell and Zachos, 2016). The current CO_2 emissions are ten times faster than at any point in the last 66 million years (Zeebe, Ridgwell and Zachos, 2016). To set the boundary conditions and tipping points of modern global warming, benchmark forecasts of future climate rely on the information of past environmental conditions and climate systems by using proxies (Rohling *et al.*, 2012; Friedrich and Timmermann, 2020). Such paleoclimate reconstructions highlight key global-warming events throughout geological time, which are often evoked as potential analogs for future climate conditions (e.g., Burke *et al.*, 2018; Haywood *et al.*, 2019; - Tierney *et al.*, 2020).

Among these analogs, the Miocene Climatic Optimum (MCO; 15.97 – 11.61 Ma) stands out as a greenhouse interval that mirrors near-future climate scenarios (Steinthorsdottir *et al.*, 2020) due to its higher temperatures (~7 to 8 °C warmer; Lear, Elderfield and Wilson, 2000; Markwick and Valdes, 2004; You *et al.*, 2009; Utescher *et al.*, 2011; Reichgelt *et al.*, 2013; Zhang *et al.*, 2013; Zhang, Pagani and Liu, 2014; Pound and Riding, 2016) and CO_2 levels than today (Beerling and Royer, 2011; Foster, Lear and

Rae, 2012; Zhang *et al.*, 2013; Super *et al.*, 2018; Sosdian *et al.*, 2020; Steinthorsdottir, Jardine and Rember, 2020). The MCO's maximum CO_2 values are synchronous with volcanic degassing of the Columbia River Basalts Group (CRBG), which is interpreted as one of its triggering factors (Hodell and Woodruff, 1994; Foster, Lear and Rae, 2012; McKay *et al.*, 2014; Kasbohm and Schoene, 2018). Although the paleoenvironmental reconstruction of this event has offered new insights on how climate may operate in the future, MCO models have failed to reconcile the decoupling between temperature and atmospheric CO_2 levels (You *et al.*, 2009; Greenop *et al.*, 2014). The proxy record shows protracted global warming at ca. 16-15 Ma, which reaches up to 6°C above the background temperature for early Miocene (You *et al.*, 2009; Greenop *et al.*, 2014); but CO_2 levels lower than 800 ppm could not sustain such warm temperature (Greenop *et al.*, 2014). The mismatch of these conditions emphasizes the challenges in using past climate systems as predictors of future climate.

The construction, assessment, and calibration of climate models addressing past systems are based on the proxy record obtained from marine sedimentary archives, which frequently represent long timescales spanning millions of years. The slow sedimentation rates, typical for oceanic basins, form records that can be tuned by orbital cycles ranging from 20 to 400 thousand years (Zachos *et al.*, 2001). Although these timescales offer valuable insights about climate variability forced by orbital precession, obliquity, and eccentricity (e.g., Berger and Loutre, 1994), their resolution is not compatible with environmental changes in human time scales. Although available paleoclimate records define long-term trends (Zachos *et al.*, 2001; Cramer *et al.*, 2009), they preclude a

comparison between the deep geological past and the climate in the next years, decades, and centuries due to the scarcity of high-resolution paleoclimate archives. Thus, identifying and reconstructing the sedimentary history of high-resolution sedimentary records – spanning from annual to millennial resolution – becomes paramount to establish analogies between past key climate events and future climate conditions (Zolitschka *et al.*, 2015; Schimmelmann *et al.*, 2016).

Varved lake sediments are a prime example of high-resolution records because they offer paleoenvironmental archives embedded into varve structures that function as temporal markers based on their thickness (Zolitschka *et al.*, 2015). Varves are commonly preserved in modern temperate and high latitudinal lake deposits (Zolitschka *et al.*, 2015) and found throughout the geological record, such as the world-famous Eocene Green River Formation in the USA (Anderson and Dean, 1988). These structures are marked by the intercalation of laminae, which is formed by shifts in the sediment accumulation in the lacustrine environment due to seasonal changes in hydrological patterns (Anderson, 1996; Zolitschka *et al.*, 2015). The detrital material deposited into the lake catchment area forms interleaved, distinguishable sub-millimetric to centimetric layers (Anderson, 1996; Zolitschka *et al.*, 2015). The rhythmic changes in color, grain size, and composition among these layers are translated into seasonal events, representing a floating chronology denominated as varve-years (Anderson, 1996; Zolitschka *et al.*, 2015).

The Clarkia Lake Deposit in northern Idaho, USA, is a world-renowned *Lagerstätte* formed by the damming of the proto St. Maries river by the Columbia River Flood Basalt Group volcanism in the MCO (Smiley, Gray and Huggins, 1975; Smiley and

Rember, 1981, 1985b). Its varved sedimentary sequence, which contains exquisitely preserved plant fossils (Smiley and Rember, 1981, 1985a) is attributed to a long-term geomorphologic stability under seasonal climate (Zolitschka *et al.*, 2015). Despite being studied since the late 1970s, the temporal framework of the Clarkia Lake Deposit has only been defined as early to middle Miocene based on paleontological evidence and tephrochronology relations (Smiley, Gray and Huggins, 1975; Smiley and Rember, 1981, 1985b; Smith and Elder, 1985; Nash and Perkins, 2012; Ladderud *et al.*, 2015). Thus, establishing chronological markers given by direct radiometric dating and floating chronology from varve years are fundamental steps to employ the Clarkia Lake Deposit as an annually-resolved sedimentary archive of a key global warming event – the MCO.

My thesis study offers the first U-Pb zircon ages obtained from ash-layers of the Clarkia Lake deposit, anchoring its deposition to 15.78 ± 0.03 Ma, synchronous to the Wanapum Formation (cf. Kasbohm and Schoene, 2018), at the end of intense eruption phases of the CRBG. Also, the calculation of varve-years in the age model for the Clarkia sediments was based on elemental and color variation ratios obtained from spectral analysis of micro X-ray fluorescence data as well as petrographic evidence. Using both approaches to establish a stratigraphic relation hip for the Clarkia Lake Deposit, the ~7.5 m thick varved sediments represent ~840 years during the MCO. By successfully setting the Clarkia Lake Deposit to the MCO, this study offers a unique opportunity to frame climate studies of the warmest phase of the entire Neogene on an unprecedented resolution.

2. ANNUALLY-RESOLVED SEDIMENTS IN THE CLASSIC CLARKIA LACUSTRINE DEPOSITS DURING THE MIDDLE MIOCENE CLIMATE OPTIMUM*

2.1. Overview

The world-renowned Miocene Clarkia Lake in northern Idaho (USA) is closely associated with the CRBG volcanism. The flood basalt dammed a local drainage system to form the paleolake, which preserved a plant fossil *Lagerstätte* in its deposits. However, the precise age and temporal duration of the lake remain unsettled. Here we present the first unequivocal U-Pb zircon ages from interbedded volcanic ashes at the P-33 type location, constraining the deposition to 15.78 ± 0.039 Ma. Using micro X-Ray fluorescence, petrographic and spectral analyses, we establish the annual characteristics of laminations throughout the stratigraphic profile by distributing elemental ratios, mineral assemblages, grain-size structures, as well as organic and fossil contents. Consequently, the ~7.5 m thick varved deposit at the classic P-33 site represents ~840 years of deposition, coincident with the end of the main-phase of CRBG eruptions during the MCO. The timing and temporal resolution of the deposit offer a unique opportunity to study climate change at an unprecedented detail during global warming associated with carbon cycle perturbations.

*Reprinted with permission from "**Annually-resolved sediments in the classic Clarkia lacustrine deposits (Idaho USA) during the middle Miocene Climate Optimum**", by Daianne Höfig, Yi Ge Zhang, Liviu Giosan, Qin Leng, Jiaqi Liang, Mengxiao Wu, Brent Miller, and Hong Yang, 2021. *Geology*, in press, Copyright 2021 by Geological Society of America. The original manuscript format is retained.

2.2. Introduction

Lava flows from the CRBG dammed the proto-St. Maries River in present-day northern Idaho, USA (Fig. 1A), creating the Clarkia paleolake in a steep-sided narrow valley (Fig. 1B; Smiley and Rember, 1985b). Despite being studied for almost five decades for its exquisitely preserved fossil biota, biomolecules, and isotope signals (Yang and Huang, 2003 and references therein), a precise temporal framework of this classic Cenozoic lacustrine deposit remains elusive due to the lack of direct radiometric ages and unresolved sedimentation rates. Early paleobotanical studies suggested that the Clarkia floras are early to middle Miocene (Smiley and Rember, 1981, 1985a). The type locality of the deposit, Site P-33 (46°59'29.5"N 116°16'35.2"W, Fig. 1C), contains ash layers tephrochronologically correlated to other ash beds in the Pacific Northwest dated between 16 and 15.4 Ma (Nash and Perkins, 2012; Ladderud *et al.*, 2015). These ages correspond to the MCO, a global warming event marked by the maximum $\delta^{13}C$ and minimum $\delta^{18}O$ benthic foraminiferal values over the past 23 Ma (Zachos *et al.*, 2001). The MCO had high atmospheric CO_2 levels attributed by some to volcanic outgassing in the CRBG (Hodell and Woodruff, 1994; Foster, Lear and Rae, 2012; Zhang *et al.*, 2013; Kasbohm and Schoene, 2018). An initial debate regarding whether the laminated sedimentary structures represent rapid deposition due to frequent storm events (Smiley and Rember, 1981) or reflect seasonal variations (Smith and Elder, 1985) has precluded the establishment of a timeframe for the Clarkia deposits.

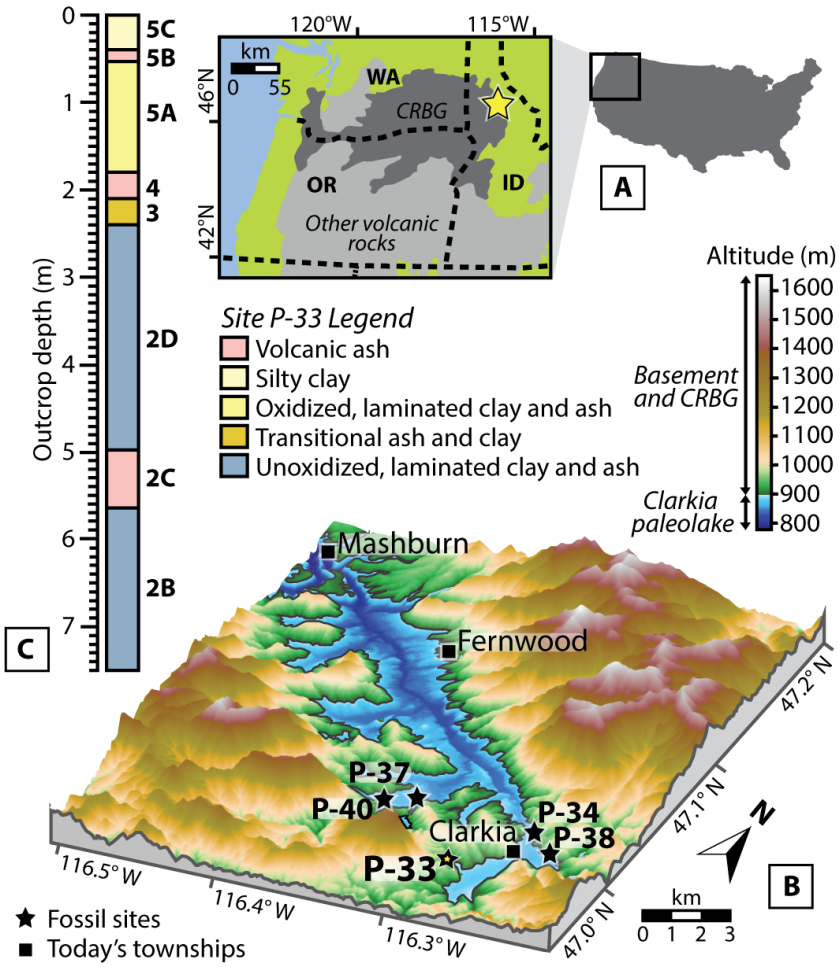

Figure 1 - Location of the Clarkia Lake Deposit. A) Location of the Clarkia deposit (modified from Wang *et al.*, 2017). CRBG stands for the Columbia River Basalt Group. B) Topographic elevation model of the Clarkia paleolake during the middle Miocene (area ca. 126 km2 based on Smiley and Rember, 1985a descriptions). C) Stratigraphic profile of Site P-33 (updated from Smiley and Rember, 1985a). Reprinted from Höfig *et al.* (2021).

Precise sedimentation rates for Clarkia deposits coupled with radiometric dating on their volcanic ashes can constrain the sedimentary–volcanic–climatic relations within the Columbia Plateau. They offer a chronological framework to investigate global climate and carbonate cycle perturbations during the warmest phase of the entire Neogene. Also, establishing an age model based on the sedimentation rates at Site P-33 can provide

insights into the development and preservation of the world-renowned fossil *Lagerstätte* that has served as both a source of material for the discovery of ancient biomolecules and a test bed for the application of new technology over several decades (e.g., Yang and Huang, 2003; Wang *et al.*, 2017).

Here we present the first U-Pb zircon ages of volcanic ash layers interbedded in the P-33 deposit. Also, by applying micro X-ray fluorescence (μ-XRF) spectral analysis of elemental distribution, we tie the laminated deposit to annual- to centennial-scale sedimentary processes during the MCO. Our data contextualize the Clarkia paleolake in a millennium timeframe at the end of the primary phase of CRBG eruptions (Kasbohm and Schoene, 2018), with elevated greenhouse gas levels, and global warming (Hodell and Woodruff, 1994; McKay *et al.*, 2014; Kasbohm and Schoene, 2018; Sosdian *et al.*, 2020).

2.3. Methods

U-Pb zircon ages of the ash layers (units 2C, 4 and 5B, Fig. 1C) were obtained via laser ablation inductively coupled plasma mass spectrometry (LA-ICP-MS) and chemical abrasion isotope dilution thermal ionization mass spectrometry (CA-ID-TIMS) at three different labs (University of Arizona, USA; Texas A&M University, USA; and China University of Geosciences at Wuhan, China). Sedimentation rates were determined using sediment block samples from units 2B, 2D, and 5A at Site P-33 (Fig. 1C). Mineralogical and textural aspects of the laminated sediments were assessed via thin-section petrography and paired with μ-XRF data. The latter were processed using spectral analysis to detect changes in the grain-size and elemental distribution along with the laminated structures.

Detailed methodology and analytical procedures are provided in the Appendixes A and B. The U-Pb zircon and μ-XRF data raw data used here are found in a Supplementary File available with this thesis.

2.4. Radiometric Ages of the P-33 Volcanic Ash Layers

LA-ICP-MS U-Pb zircon ages from the tephra layers 2C, 4, and 5B are geochronological markers for Site P-33 (Fig. 2).

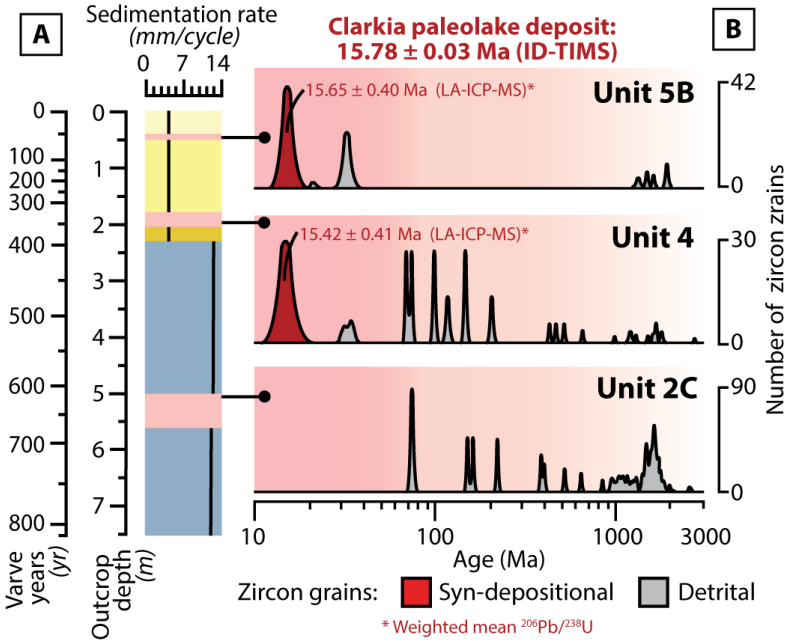

Figure 2 - Proposed age model for the Clarkia paleolake. A) Varve years were determined using the average values of the sedimentation rates (vertical lines within the column), each unit's thickness, and outcrop height. The legend is the same as Fig. 1. B) Probability density diagrams of U-Pb zircon ages (LA-ICP-MS) from units 2C, 4, and 5B. Reprinted from Höfig *et al.* (2021).

For units 2C, 4, and 5B, concordant detrital ages range from 74.0 ± 1.3 to 2533.5 ± 17 Ma, 14.0 ± 1 to 2704.5 Ma, and 15.07 ± 0.46 to 1914.7 ± 14.2 Ma,

respectively. Miocene volcanogenic populations, identified in units 4 and 5B, have a weighted mean $^{206}Pb/^{238}U$ of 15.42 ± 0.41 Ma (MSWD=1.8; n=20) and 15.65 ± 0.40 Ma (MSWD=1.9; n=23), respectively, which are interpreted as the time of zircon crystallization (Fig. B1, Appendix B). Zircon crystals identified as belonging to the Miocene population in Unit 5B were removed from the LA-ICP-MS grain mount for CA-ID-TIMS analysis, which yielded a weighted mean $^{206}Pb/^{238}U$ age of 15.85 ± 0.03 Ma (MSWD=4.6; n=14). Although the $^{206}Pb/^{238}U$ ages are over-dispersed, all analyses are concordant, and there is no clear basis for excluding analyses at either end of the distribution. We interpret the youngest, high-resolution CA-ID-TIMS age of 15.78 ± 0.035/0.035/0.039 (uncertainties listed in order of analytical / including tracer / including decay constants) from the Unit 5B ash (analysis #12) as the timing of zircon crystallization and the best estimate for the age of volcanism at this level in the Clarkia deposit at Site P-33. Although Unit 5B overlies Unit 4 (15.42 ± 0.41 Ma), the proposed duration of the entire section, less than 1000 years (see below), is well outside the resolution of U-Pb dating methods. The U-Pb data presented here are mainly to place the Clarkia volcanic deposits within the temporal framework of the CRBG (cf. Kasbohm and Schoene, 2018). The bottommost ash layer, Unit 2C, does not yield Miocene volcanogenic ages, and groundmass separates of the volcanic material show only a few rounded zircon grains (Fig. B2, Appendix B) and abundant glass shards. These features are strong evidence of reworking of much older material from the region during deposition.

A previous study correlated chemical signatures of volcanic glass shards and tephras of Unit 4 with the Cold Springs Tuff in Nevada volcanic field with a known age

between 15.85 ± 0.16 Ma and 15.50 ± 0.08 Ma (Brueseke and Hart, 2008; ± 2σ relative to Fish Canyon Sanidine recalculation by Ladderud *et al.*, 2015). There is also a potential connection between the Unit 2C and Bully Creek Formation's tuff in Oregon (15.66 ± 0.07 Ma; Downing and Swisher, 1993; Nash and Perkins, 2012). The 15.78 ± 0.039 Ma zircon age for the Clarkia deposit agrees with previous chronology established through paleobotanical data and tephra correlations.

2.5. Annually Resolved Sedimentation Rates

Except for the ash layers, sediments show laminations of fining-upward couplets throughout the succession at Site P-33. Their chemical and mineral compositions, grain-size structures, and fossil content strongly suggest that these laminations represent annual rhythmicity in depositional records (i.e., varved structures; Fig. B3A-B, Appendix B). P-33 laminations show intercalation of dark, fine-grained, fossil-rich layers and light, coarse-grained, fossil-barren layers. In the lower portion of the outcrop, defined as the unoxidized zone (units 2B and 2D; Fig. 1C), petrographic thin section analysis revealed that couplets in the dark gray laminated clays are mineralogically very similar but vary in grain-size and proportions of detrital minerals (Fig. B3C, Appendix B). In this zone, well-preserved fossil leaf compressions are only found in the fine-grained lamina (Fig. B3D, Appendix B). The fining-upward sequence suggests that the suspended sediment brought by seasonal runoff was segregated by density into a stratified water body. Coarser, denser particles are likely to deposit in the growth season (i.e., spring and summer), and finer particles are suspended in the water column, settling at lower rates in the deciduous season (i.e., autumn

and winter) along with abundant deciduous plant leaves to complete an annual depositional cycle. In the upper portion of the outcrop, the oxidized zone (units 5A to 5C; Figs. 1C and B3E, Appendix B) presents less fossil content than units below, mostly as leaf impressions. The cryptocrystalline texture of the ashfall layers (units 2C, 4, and 5B) hindered the petrographic assessment of these samples (Fig. B3F, Appendix B).

Spectral analysis of elemental distribution in the unoxidized and oxidized zones shows rhythmic cycles coherent with the varve structures observed in the block samples and thin sections (Figs. 3 and B4-5, Appendix B). Element ratios traditionally attributed to grain-size variation (K/Ti and Rb/Zr) concur with changes in the lamination thickness, commonly seen in varves (e.g., Palmer *et al.*, 2019). Titanium and zirconium represent sand-sized material input, enriched in heavy minerals, while potassium and rubidium reflect clay minerals and micas in the fine-grained fractions (Dypvik and Harris, 2001; Chen *et al.*, 2006; Hennekam and de Lange, 2012). Power spectra of red-color intensity transect across the varves (color*) represents color changes in scanned images from varve structures (Fig. 3). Organic content is detected by the Compton and Rayleigh counts (Inc/Coh), in which the augmented intensity of incoherent scatter at an energy level is lower than the tube-anode radiation (Thomson, Croudace and Rothwell, 2006). Higher Inc/Coh ratios correspond to the fine-grained, fossil-rich layers in the varved sediments (Figs. 3 and B4-5, Appendix B). These matching changes of grain-size, color, and fossil content occur at every ~1 cm in the unoxidized zone and 0.5 cm in the oxidized zone (Figs. 3 and BR4-5, Appendix B), a variation of varve thickness that is within the range of documented varved sediments (Zolitschka *et al.*, 2015).

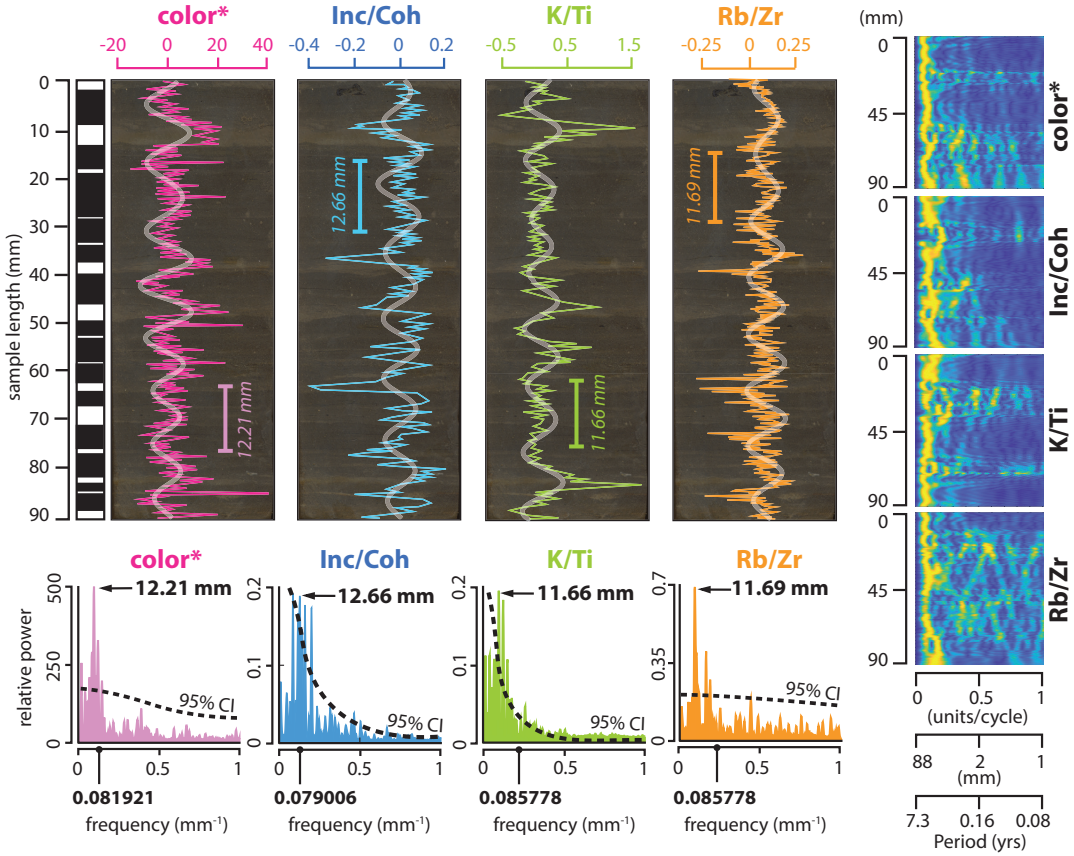

Figure 3 - Spectral analysis. Frequency analysis of color*, Inc/Coh, K/Ti, and Rb/Zr reveals the interval of depositional cycles in Unit 2B. All data are detrended and normalized. Signals of depositional cycles stand out above the 95% confidence interval in the power spectra and the Fast Fourier Transform processing (light-colored bands). Reprinted from Höfig *et al.* (2021).

The Clarkia plant fossil assemblage, characterized by deciduous species reflecting a mixed mesophytic flora developed in a warm temperate climate with strong seasonality (Smiley and Rember, 1985b), indicates a climate regime that favored deposits with seasonal rhythms. The excellent preservation of plant fossils in laminated Clarkia sediments (Smiley and Rember, 1985b) and the absence of bioturbation (Smith and Elder, 1985) attest to sustained lake stratification with anoxic hypolimnion conditions (Fig. 4).

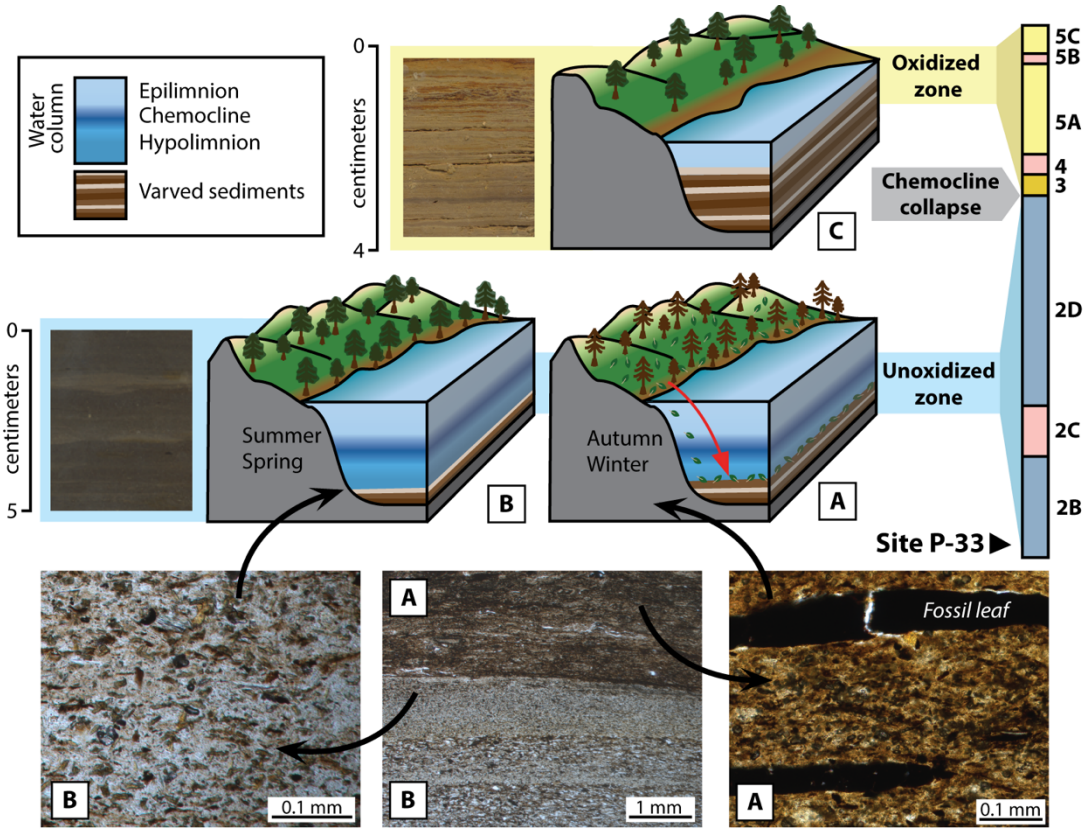

Figure 4 - Evolution model of the Clarkia deposit at Site P-33. In the open-lake phase, during autumn and winter, leaves shed from surrounding trees are deposited and preserved in dark, fine-grained layers (A). These layers were interleaved with fossil-barren, coarse-grained layers deposited during the spring and summer (B). As the drainage system changed (Unit 3), likely by rupture of the basalt dam holding the lake reservoir, the chemocline collapsed, leading to a shallow and oxidized environment with reduced depositional rates (C). Reprinted from Höfig *et al.* (2021).

2.6. The Clarkia Age Model and Implications

Evidence of varved structures found throughout the P-33 section and their rate variation is crucial to reconstruct an age model associated with the change of depositional environments for the Clarkia deposit (Fig. 2A). Assuming similar rates for the transitional Unit 3 and instantaneous deposition of autochthonous ash layers (e.g., Units 4 and 5B),

the ~7.5 m sedimentary sequence at Site P-33 corresponds to approximately 840 varve years at the end of the primary phase of CRBG eruptions (Fig. 2). The U-Pb ages from the ash layers, although not precise enough to calibrate the age model, do help to place the Clarkia deposits into the overall temporal framework of CRBG eruption. The age model has strong implications for Clarkia paleolake's evolutionary history, the exceptional preservation of fossil material, and the middle Miocene CO_2 pulse.

The interpretation of laminated Clarkia sediments as recording seasonality is favored over the storm hypothesis due to the tight coupling between the grain-size change and fossil abundance. Abundant deciduous leaves within the fine-grained autumn sediments are consistent with rhythmic seasonal deposition of varves. While both storm deposits and dammed lakes may result in high sedimentation rates (Glenn and Kelts, 1991), irregular storms and floods tend to create turbulence that disturbs lake stratification and destroys laminations and fossil material, which contradicts the existing evidence.

Rapid burial in stratified lakes is a critical controlling factor for the exceptional preservation of organic fossils (Seilacher, Reif and Westphal, 1985; Briggs, 2003). The accumulation rate in the unoxidized zone (~12 mm/year) is considered fast for varve formation in a stratified lake (Zolitschka *et al.*, 2015), preventing the decay of organic matter and forming high-quality leaf compressions with intact tissues and biomolecules (*Konservat-Lagerstätte*). Shifts in sedimentation rates at Site P-33 detected via spectral analysis of μ-XRF data (Figs. 3, B4-5, Appendix B) are consistent with the proposed sudden changes in the drainage system leading to shallowing of the Clarkia paleolake, ending the lake stratification, and transforming it into a polymictic mixing regime (Fig.

4C; Wang *et al.*, 2017). After the reconfiguration of the lake, the sedimentation rate becomes much lower (~6 mm/year) in an oxidized, shallow, and ventilated water column that favors the preservation of leaf impressions (*Konzentrat-Lagerstätte*) with the same vegetation input (Wang *et al.*, 2017).

Our new Miocene U-Pb zircon ages obtained from the Clarkia paleolake are synchronous with the Priest Rapids Member from the Wanapum Basalt Formation of the CRBG (15.895 ± 0.019 Ma; Kasbohm and Schoene, 2018). It was formed after the peak of CRBG eruption which produced a volume of basalt of 12,175 km^3 (Kasbohm and Schoene, 2018) associated with some 240-280 Pg of carbon release to the atmosphere. Vigorous volcanism is also a potential driver for the positive excursions of benthic $\delta^{13}C$ during the MCO (Armstrong McKay et al., 2014; Kasbohm and Schoene, 2018; Sosdian et al., 2020). Fluctuations of CO_2 on orbital timescale during the Miocene are large, above 100-200 ppm, as documented by boron isotope records (Greenop *et al.*, 2014). We speculate that some of these high amplitude changes could be attributed to volcanic CO_2 release and its subsequent consumption. The better-constrained age and temporal resolution of the Clarkia deposits will aid future tests of this hypothesis. Our results provide the first absolute age constraint for the Clarkia *Lagerstätte* that confined the exceptional biomolecular preservation in annually resolved sediments at P-33 within a millennium during the MCO, framing a unique Neogene window for future research on the interactions of volcanism, climate, and terrestrial ecosystem.

3. CONCLUSIONS

This thesis provides a temporal framework for the Clarkia Lake Deposit in relation to the CRBG eruption history, establishing it as a high-resolution paleoenvironmental archive of the MCO. A multitechnique approach was employed to define the age and sedimentation history of Site P-33. The age was determined using U-Pb zircon dating of three ash layers of the Clarkia Lake Deposit (units 2C, 4, and 5B) via LA-ICP-MS and CA-ID-TIMS in three different laboratories. The youngest, most precise age of 15.78 ± 0.03 Ma in the Unit 5B places the Clarkia Lake Deposit to the middle Miocene. Petrographic analysis of thin-sections from the varved sediments (units 2B, 2D, and 5A) emphasize the varve structures observed in the Site P-33 outcrop. The interleaved dark, fine-grained, fossil-rich layers and the light, coarse-grained, fossil-barren layers are strong evidence of seasonal deposition. The sedimentation rates, calculated using spectral analysis of μ-XRF data representing grain-size variation (K/Ti and Rb/Zr) along the varve structures, corroborates the annually-resolved deposition.

The physical setting of the Clarkia *Lagerstätte* is reconstructed using changes in the sedimentation rates, lithology, and fossil preservation along the Site P-33. The unoxidized zone (units 2A, 2B, 2D) has sedimentation rate of ~1 cm/year, which attests to favorable conditions of fossil preservation, such as stratification of the water column and anoxic bottom water. The presence of exquisitely preserved flora in the dark, fine-grained layers of the varve structures attributes the status of *Konservat* deposit for the bottom part of the Site P-33. Changes of the lake dynamic are given by Unit 3, which has

coarse-grained sediments that are poorly laminated and destitute of fossil flora. Wang *et al.* (2017) interpret this layer as representing rapid shallowing of the lake, possibly due to the collapse of the lava-flow dam holding the proto St. Maries River. The oxidized zone (units 5A and 5C) has sedimentation rate of ~ 0.5 cm/year, which denotes poor conditions of fossil preservation, such as ventilation of the water column and lake shallowing. Fossil flora are commonly found as compressions in this zone, defining *Konzentrat* deposit.

The age model based on the calculated sedimentation rates for the Clarkia Lake Deposit establishes that the ~ 7.5 m sedimentary sequence of the Site P-33 represent ca. 840 years. The implications of this finding are manifold. Firstly, it opens an opportunity to contextualize paleoclimate studies using of the samples from the Clarkia Lake Deposit into a precise timeframe of the CRBG development. With this geochronological marker, paleoclimate reconstructions of the MCO employing samples from the Clarkia Lake Deposit, will represent intervals equivalent to the human lifespan timescale. Such records strengthen the past climate systems as analogs for future climate conditions, enabling the calibration of benchmark climate models, for example. Also, the Clarkia Lake Deposit is a snapshot of the warmest phase of Neogene, containing a wealth of proxy record that can shed light on the MCO conundrum of CO_2 and temperature decoupling (cf. You *et al.*, 2009; Greenop *et al.*, 2014).

REFERENCES

Anderson, R. Y. (1996) 'Seasonal sedimentation: a framework for reconstructing climatic and environmental change', *Geological Society, London, Special Publications*, 116(1), pp. 1–15. doi: 10.1144/GSL.SP.1996.116.01.02.

Anderson, R. Y. and Dean, W. E. (1988) 'Lacustrine varve formation through time', *Palaeogeography, Palaeoclimatology, Palaeoecology*. doi: 10.1016/0031-0182(88)90055-7.

Barr, S. M. *et al.* (2019) 'Detrital zircon signatures in Precambrian and Paleozoic sedimentary units in southern New Brunswick – more pieces of the puzzle', *Atlantic Geology*, 55, pp. 275–322. doi: 10.4138/atlgeol.2019.010.

Beerling, D. J. and Royer, D. L. (2011) 'Convergent Cenozoic CO_2 history', *Nature Geoscience*, 4(7), pp. 418–420. doi: 10.1038/ngeo1186.

Berger, A. and Loutre, M. F. (1994) 'Precession, Eccentricity, Obliquity, Insolation and Paleoclimates', in *Long-Term Climatic Variations*. doi: 10.1007/978-3-642-79066-9_5.

Briggs, D. E. G. (2003) 'The role of decay and mineralization in the preservation of soft-bodied fossils', *Annual Review of Earth and Planetary Sciences*. doi: 10.1146/annurev.earth.31.100901.144746.

Brueseke, M. E. and Hart, W. K. (2008) 'Geology and Petrology of the Mid-Miocene Santa Rosa-Calico Volcanic Field, Northern Nevada', *Nevada Bureau of Mines and Geology*. Reno, Bulletin 1.

Burke, K. D. *et al.* (2018) 'Pliocene and Eocene provide best analogs for near-future climates', *Proceedings of the National Academy of Sciences of the United States of America*. doi: 10.1073/pnas.1809600115.

Charney, J. G. *et al.* (1979) *Carbon Dioxide and Climate: A scientific assessment*. Washington, D.C.: National Academy of Sciences. doi: 10.17226/12181.

Chen, J. *et al.* (2006) 'Zr/Rb ratio in the Chinese loess sequences and its implication for changes in the East Asian winter monsoon strength', *Geochimica et Cosmochimica Acta*, 70(6), pp. 1471–1482. doi: 10.1016/j.gca.2005.11.029.

Condon, D. J. *et al.* (2015) 'Metrology and traceability of U–Pb isotope dilution geochronology (EARTHTIME Tracer Calibration Part I)', *Geochimica et Cosmochimica Acta*, 164, pp. 464–480. doi: 10.1016/j.gca.2015.05.026.

Cramer, B. S. *et al.* (2009) 'Ocean overturning since the Late Cretaceous: Inferences from

a new benthic foraminiferal isotope compilation', *Paleoceanography*, 24(4). doi: 10.1029/2008PA001683.

Croudace, I. W., Rindby, A. and Rothwell, R. G. (2006) 'ITRAX: Description and evaluation of a new multi-function X-ray core scanner', *Geological Society Special Publication*. doi: 10.1144/GSL.SP.2006.267.01.04.

Downing, K. F. and Swisher, C. C. (1993) 'New $^{40}Ar/^{39}Ar$ Dates and Refined Geochronology of the Sucker Creek Formation, Oregon', in *Abstracts of Papers*. Alburquerque, New Mexico: Jounal of Vertebrate Paleontology, p. A33.

Dypvik, H. and Harris, N. B. (2001) 'Geochemical facies analysis of fine-grained siliciclastics using Th/U, Zr/Rb and (Zr+Rb)/Sr ratios', *Chemical Geology*, 181(1–4), pp. 131–146. doi: 10.1016/S0009-2541(01)00278-9.

Foster, G. L., Lear, C. H. and Rae, J. W. B. (2012) 'The evolution of pCO_2, ice volume and climate during the middle Miocene', *Earth and Planetary Science Letters*. doi: 10.1016/j.epsl.2012.06.007.

Friedrich, T. and Timmermann, A. (2020) 'Using Late Pleistocene sea surface temperature reconstructions to constrain future greenhouse warming', *Earth and Planetary Science Letters*, 530, p. 115911. doi: 10.1016/j.epsl.2019.115911.

Gehrels, G. E., Valencia, V. A. and Ruiz, J. (2008) 'Enhanced precision, accuracy, efficiency, and spatial resolution of U-Pb ages by laser ablation-multicollector-inductively coupled plasma-mass spectrometry', *Geochemistry, Geophysics, Geosystems*, 9(3), pp. 1–13. doi: 10.1029/2007GC001805.

Glenn, C. and Kelts, K. (1991) 'Rhythms in lacustrine deposits', in Einsele, G., Ricken, W., and Seilacher, A. (eds) *Cyclic and Event Stratigraphy*. Berlin: Springer-Verlag, pp. 188–221.

Greenop, R. *et al.* (2014) 'Middle Miocene climate instability associated with high-amplitude CO_2 variability', *Paleoceanography*. doi: 10.1002/2014PA002653.

Haywood, A. M. *et al.* (2019) 'What can Palaeoclimate Modelling do for you?', *Earth Systems and Environment*. doi: 10.1007/s41748-019-00093-1.

Hennekam, R. and de Lange, G. (2012) 'X-ray fluorescence core scanning of wet marine sediments: methods to improve quality and reproducibility of high-resolution paleoenvironmental records', *Limnology and Oceanography: Methods*, 10(12), pp. 991–1003. doi: 10.4319/lom.2012.10.991.

Hodell, D. A. and Woodruff, F. (1994) 'Variations in the strontium isotopic ratio of

seawater during the Miocene: Stratigraphic and geochemical implications', *Paleoceanography*, 9(3), pp. 405–426. doi: 10.1029/94PA00292.

Höfig, D. F. *et al.* (2021) 'Annually-resolved sediments in the classic Clarkia lacustrine deposits (Idaho USA) during the middle Miocene Climate Optimum', *Geology*, (in press).

Kasbohm, J. and Schoene, B. (2018) 'Rapid eruption of the Columbia River flood basalt and correlation with the mid-Miocene climate optimum', *Science Advances*, 4(9). doi: 10.1126/sciadv.aat8223.

Ladderud, J. A. *et al.* (2015) 'Volcanic Ash Layers in the Miocene Lake Clarkia Beds: Geochemistry, Regional Correlation, and Age of the Clarkia Flora', *Northwest Science*, 89(4). doi: 10.3955/046.089.0402.

Lear, C. H., Elderfield, H. and Wilson, P. (2000) 'Cenozoic Deep-Sea Temperatures and Global Ice Volumes from Mg/Ca in Benthic Foraminiferal Calcite', *Science*, 287(5451), pp. 269–272. doi: 10.1126/science.287.5451.269.

Li, M., Hinnov, L. and Kump, L. (2019) 'Acycle: Time-series analysis software for paleoclimate research and education', *Computers & Geosciences*, 127, pp. 12–22. doi: 10.1016/j.cageo.2019.02.011.

Ludwig, K. R. (2003) *User's manual for Isoplot 3.00, a geochronological toolkit for Microsoft Excel. Berkeley Geochronology Center special publication no.4*, *Components*.

Mann, M. E. and Lees, J. M. (1996) 'Robust estimation of background noise and signal detection in climatic time series', *Climatic Change*, 33(3), pp. 409–445. doi: 10.1007/BF00142586.

Markwick, P. J. and Valdes, P. J. (2004) 'Palaeo-digital elevation models for use as boundary conditions in coupled ocean–atmosphere GCM experiments: a Maastrichtian (late Cretaceous) example', *Palaeogeography, Palaeoclimatology, Palaeoecology*, 213(1–2), pp. 37–63. doi: 10.1016/j.palaeo.2004.06.015.

Mattinson, J. M. (2005) 'Zircon U–Pb chemical abrasion ("CA-TIMS") method: Combined annealing and multi-step partial dissolution analysis for improved precision and accuracy of zircon ages', *Chemical Geology*, 220(1–2), pp. 47–66. doi: 10.1016/j.chemgeo.2005.03.011.

McKay, D. I. A. *et al.* (2014) 'Estimating the impact of the cryptic degassing of Large Igneous Provinces: A mid-Miocene case-study', *Earth and Planetary Science Letters*, 403, pp. 254–262. doi: 10.1016/j.epsl.2014.06.040.

Miller, B. V. *et al.* (2018) 'Tonian Fe-Ti-P ferronorite and alkali anorthosite in the

northern Appalachian orogen, southern New Brunswick, Canada: Amazonian basement in Ganderia?', *Precambrian Research*. doi: 10.1016/j.precamres.2018.08.006.

Muller, R. A. and MacDonald, G. J. (2000) *Ice Ages and Astronomical Causes: Data, Spectral Analysis, and Mechanisms*. Berlin: Springer-Verlag Berlin Heidelberg.

Nash, B. P. and Perkins, M. E. (2012) 'Neogene Fallout Tuffs from the Yellowstone Hotspot in the Columbia Plateau Region, Oregon, Washington and Idaho, USA', *PLoS ONE*. doi: 10.1371/journal.pone.0044205.

Palmer, A. P. *et al.* (2019) 'The micromorphology of glaciolacustrine varve sediments and their use for reconstructing palaeoglaciological and palaeoenvironmental change', *Quaternary Science Reviews*. doi: 10.1016/j.quascirev.2019.105964.

Park, A. F. *et al.* (2014) 'Structural setting and age of the partridge island block, southern New Brunswick, Canada: A link to the Cobequid highlands of northern mainland Nova Scotia', *Canadian Journal of Earth Sciences*. doi: 10.1139/cjes-2013-0120.

Pound, M. J. and Riding, J. B. (2016) 'Palaeoenvironment, palaeoclimate and age of the Brassington Formation (Miocene) of Derbyshire, UK', *Journal of the Geological Society*, 173(2), pp. 306–319. doi: 10.1144/jgs2015-050.

Reichgelt, T. *et al.* (2013) 'Quantitative palaeoclimate estimates for Early Miocene southern New Zealand: Evidence from Foulden Maar', *Palaeogeography, Palaeoclimatology, Palaeoecology*, 378, pp. 36–44. doi: 10.1016/j.palaeo.2013.03.019.

Rohling, E. J. *et al.* (2012) 'Making sense of palaeoclimate sensitivity', *Nature*. doi: 10.1038/nature11574.

Schimmelmann, A. *et al.* (2016) 'Varves in marine sediments: A review', *Earth-Science Reviews*, 159, pp. 215–246. doi: 10.1016/j.earscirev.2016.04.009.

Schmitz, M. D. and Schoene, B. (2007) 'Derivation of isotope ratios, errors, and error correlations for U-Pb geochronology using ^{205}Pb- ^{235}U-(^{233}U)-spiked isotope dilution thermal ionization mass spectrometric data', *Geochemistry, Geophysics, Geosystems*, 8(8), p. n/a-n/a. doi: 10.1029/2006GC001492.

Seilacher, A., Reif, W. E. and Westphal, F. (1985) 'Sedimentological, ecological and temporal patterns of fossil Lagerstatten.', *Extraordinary fossil biotas: their ecological and evolutionary significance*. doi: 10.1098/rstb.1985.0134.

Smiley, C. J., Gray, J. and Huggins, L. M. (1975) 'Preservation of Miocene Fossils in Unoxidized Lake Deposits, Clarkia, Idaho; With a Section on Fossil Insecta by W. F. Barr and J. M. Gillespie', *Journal of Paleontology*. Paleontological Society, 49(5), pp. 833–

844. Available at: http://www.jstor.org/stable/1303276.

Smiley, C. J. and Rember, W. C. (1981) 'Paleoecology of the Miocene Clarkia lake (Northern Idaho)', in Gray, J., Boucot, A. J., and Berry, W. B. N. (eds) *Communities of the Past*. Stroudburg, PA, pp. 551–590.

Smiley, C. J. and Rember, W. C. (1985a) 'Composition of the Miocene Carkia flora', in Smiley, C. J. (ed.) *Late Cenozoic History of the Pacific Northwest*. San Francisco: Pacific Division of American Association for the Advancement of Science, pp. 95–112.

Smiley, C. J. and Rember, W. C. (1985b) 'Physical Setting of the Miocene Clarkia Fossil Beds, Northern Idaho', in Smiley, C. J. (ed.) *Late Cenozoic History of the Pacific Northwest*. San Francisco: Pacific Division of American Association for the Advancement of Science, pp. 11–31.

Smith, G. R. and Elder, R. D. (1985) 'Environmental Interpretation of Burial and Preservation of Clarkia Fishes', in Smiley, C. J. (ed.) *Late Cenozoic History of the Pacific Northwest*. San Francisco: Pacific Division of American Association for the Advancement of Science, pp. 85–94.

Smith, J. J. *et al.* (2018) 'First U-Pb zircon ages for late Miocene ashfall Konservat-Lagerstätte and Grove Lake ashes from eastern Great Plains, USA', *PLoS ONE*. doi: 10.1371/journal.pone.0207103.

Sosdian, S. M. *et al.* (2020) 'Ocean Carbon Storage across the middle Miocene: a new interpretation for the Monterey Event', *Nature Communications*. doi: 10.1038/s41467-019-13792-0.

Steinthorsdottir, M. *et al.* (2020) 'The Miocene: the Future of the Past', *Paleoceanography and Paleoclimatology*. doi: 10.1029/2020PA004037.

Steinthorsdottir, M., Jardine, P. E. and Rember, W. C. (2020) 'Near-Future p CO_2 during the hot Mid Miocene Climatic Optimum', *Paleoceanography and Paleoclimatology*. doi: 10.1029/2020PA003900.

Stocker, T. F. *et al.* (2013) *Climate change 2013 the physical science basis: Working Group I contribution to the fifth assessment report of the intergovernmental panel on climate change*, *Climate Change 2013 the Physical Science Basis: Working Group I Contribution to the Fifth Assessment Report of the Intergovernmental Panel on Climate Change*. doi: 10.1017/CBO9781107415324.

Super, J. R. *et al.* (2018) 'North Atlantic temperature and pCO_2 coupling in the early-middle Miocene', *Geology*, 46(6), pp. 519–522. doi: 10.1130/G40228.1.

Thomson, J., Croudace, I. W. and Rothwell, R. G. (2006) 'A geochemical application of the ITRAX scanner to a sediment core containing eastern Mediterranean sapropel units', *Geological Society Special Publication*. doi: 10.1144/GSL.SP.2006.267.01.05.

Tierney, J. E. *et al.* (2020) 'Past climates inform our future', *Science*, 370(680), pp.1-9. doi: 10.1126/science.aay3701.

Trauth, M. H. (2015) 'Time-Series Analysis', in *MATLAB® Recipes for Earth Sciences*. Berlin, Heidelberg: Springer Berlin Heidelberg, pp. 151–213. doi: 10.1007/978-3-662-46244-7_5.

Utescher, T. *et al.* (2011) 'Cenozoic climate gradients in Eurasia — a palaeo-perspective on future climate change?', *Palaeogeography, Palaeoclimatology, Palaeoecology*, 304(3–4), pp. 351–358. doi: 10.1016/j.palaeo.2010.09.031.

Wang, H. *et al.* (2017) 'A rapid lake-shallowing event terminated preservation of the Miocene Clarkia Fossil Konservat-Lagerstätte (Idaho, USA)', *Geology*, 45(3), pp. 239–242. doi: 10.1130/G38434.1.

Wiedenbeck, M. *et al.* (1995) 'Three Natural Zircon Standards For U-Th-Pb, Lu-Hf, Trace Element and REE Analyses', *Geostandards and Geoanalytical Research*, 19(1), pp. 1–23. doi: 10.1111/j.1751-908X.1995.tb00147.x.

Yancey, T. E. *et al.* (2018) 'Eocene–Oligocene chronostratigraphy of ignimbrite flareup volcanic ash beds on the Gulf of Mexico coastal plains', *Geosphere*, 14(3), pp. 1232–1252. doi: 10.1130/GES01621.1.

Yang, H. and Huang, Y. (2003) 'Preservation of lipid hydrogen isotope ratios in Miocene lacustrine sediments and plant fossils at Clarkia, northern Idaho, USA', *Organic Geochemistry*, 34(3), pp. 413–423. doi: 10.1016/S0146-6380(02)00212-7.

You, Y. *et al.* (2009) 'Simulation of the middle miocene climate optimum', *Geophysical Research Letters*. doi: 10.1029/2008GL036571.

Zachos, J. C. *et al.* (2001) 'Trends, Rhythms, and Aberrations in Global Climate 65 Ma to Present', *Science*, 292(5517), pp. 686–693. doi: 10.1126/science.1059412.

Zeebe, R. E., Ridgwell, A. and Zachos, J. C. (2016) 'Anthropogenic carbon release rate unprecedented during the past 66 million years', *Nature Geoscience*. Nature Publishing Group, 9, p. 325. doi: 10.1038/ngeo2681.

Zhang, Y. G. *et al.* (2013) 'A 40-million-year history of atmospheric CO_2', *Philosophical Transactions of the Royal Society A: Mathematical, Physical and Engineering Sciences*. doi: 10.1098/rsta.2013.0096.

Zhang, Y. G., Pagani, M. and Liu, Z. (2014) ‘A 12-Million-Year Temperature History of the Tropical Pacific Ocean’, *Science*, 344(6179), pp. 84–87. doi: 10.1126/science.1246172.

Zolitschka, B. *et al.* (2015) ‘Varves in lake sediments – a review’, *Quaternary Science Reviews*, 117, pp. 1–41. doi: 10.1016/j.quascirev.2015.03.019.

APPENDIX A

DETAILED METHODOLOGY

A1. Zircon U-Pb Geochronology

Volcanic ash samples collected from Clarkia Site P-33 were independently analyzed in three geochronology laboratories. Samples were analyzed via LA-ICP-MS in the Arizona LaserChron Center at the University of Arizona, using a Photon Machines Analyte G2 excimer laser equipped with HelEx ablation and plasma source of an Element2 HR ICPM. Imaging was carried out using a Hitachi 3400N scanning electron microscope and a Gatan CL2 detector system. Methods are as described by Gehrels *et al.* (2008). At Texas A&M University, the volcanic samples were analyzed in a Thermo Scientific™ iCAP RQ™ quadrupole mass spectrometer for LA-ICP-MS and Triton for CA-ID-TIMS at its R. Ken Williams '45 Radiogenic Isotope Geosciences Laboratory. LA-ICP-MS procedures are as detailed in Barr *et al.* (2019) and Yancey *et al.* (2018); CA-ID-TIMS procedures are described in Miller *et al.* (2018) and Park *et al.* (2014), except this study used the EarthTime 205Pb-233U-235U spike (Condon *et al.*, 2015). CA-ID-TIMS data were reduced using the "YourLab" algorithms of Schmitz and Schoene (2007). Final U-Pb age interpretations are given in the form AGE ± X/Y/Z, where AGE is the preferred age interpretation as described in the text and X, Y, Z represent the uncertainty taking into account random and systematic analytical sources (X), those combined with contributions from uncertainty in the ET535 spike (Y) and both of those and including decay constant uncertainties (Z). Corrections for ^{230}Th were performed assuming a magmatic Th/U ratio

of 3.0. At the China University of Geosciences at Wuhan, the LA-ICP-MS system consists of an Agilent7500a with a 193nm ArF-excimer laser.

Approximately 10 kg of each ash layer was collected, hand-crushed, washed, and sonicated multiple times to disaggregate clusters of glass shards and clay minerals as described by Smith *et al.* (2018). These concentrates were separated by density (hand-panning and Wifely table), magnetism (Frantz Isodynamic Magnetic Separator), and gravity (Methylene Iodine). Zircon residue was selected based on their morphology, size, color, as well as the absence of fractures, overgrowth, and inherited nuclei. For LA-ICP-MS, a dozen individual zircon grains were mounted in an epoxy stand with primary standards (NIST 612 glass and 91500 zircon), which was polished to remove surface layers affected by lead loss. For Unit 2C, 110 spots were obtained from 85 grains, yielding 85 concordant detrital ages; for Unit 4, 75 spots and grains yielded 56 concordant detrital ages (20 analyses define Miocene volcanogenic population); and for Unit 5B, 48 measurement spots out of a total of 108 on 73 grains yielded concordant ages (23 analyses define Miocene volcanogenic population). For the ID-TIMS, the selected Miocene zircon grains previously analyzed by LA-ICP-MS were dissolved in a Teflon beaker following Mattinson (Mattinson, 2005). Age calculation was performed following Wiedenbeck et al. (1995) and Concordia diagrams were obtained using Isoplot v. 247 (Ludwig, 2003).

A2. Micro X-Ray Fluorescence (μ-XRF)

Sample blocks measuring 5-9:4:2 cm (L:W:H) from the laminated units 2B, 2D, and 5A from Site P-33 were analyzed at a step size of 5 mm in the XRF Core Scanning

Facility of the IODP Gulf Coast Repository using a third-generation Avaatech XRF Core Scanner. The 27 chemical elements obtained were arranged into 702 ratio combinations, of which few ratios were shortlisted based on their reciprocity with the varve-structures and representativeness of grain-size change. To increase the resolution of the data, μ-XRF was employed on the same samples using the Cox Analytical's ITRAX XRF micro-scanner at the Woods Hole Oceanographic Institution. Elemental counts were recorded at 200-micrometer intervals using a Mo X-Ray tube set to 30 kV and 50 mA with 10 s scanning time. The XRF spectra were interpreted and the peak areas were quantified using software Q-Spec. This approach enabled data acquisition from the sub-mm varve layers of Clarkia deposit. Analytical settings follow Croudace *et al.* (2006).

Sedimentation rates were statistically estimated employing spectral analysis in the selected elemental ratios, using the Acycle 2.0 package for MATLAB (Li, Hinnov and Kump, 2019). Firstly, the dataset was filtered to remove data points affected by heterogeneities in the sample surface, such as fractures. For this procedure, argon counts and photographs were used to determine problematic areas of the sample. Then, the data set was detrended using a robust quadratic regression (rloess). Next, the time series interpretation detected cycles across the stratigraphic sample length using periodograms that show the most dominant signals (above 95% confidence interval) standing out from the background noise (Mann and Lees, 1996). Further signal processing employed evolutionary power spectra (Fast Fourier Transform) that addressed the autocorrelation of the dataset and its cyclicity (Muller and MacDonald, 2000). The data was filtered using a bandpass, assuming Gaussian distribution, to isolate the frequency representing the most

preeminent cycle (Muller and MacDonald, 2000). In addition to the XRF data acquisition, a semi-automatic image-analysis MATLAB script was used in scanned images from the samples to detect the change of the colors in the varved sediments (Trauth, 2015). Spectral analysis of the obtained color intensity transects followed the same steps as described for the μ-XRF data.

Varves are commonly preserved in modern temperate and high latitudinal lake deposits (Zolitschka *et al.*, 2015) and found throughout the geological record, such as the Eocene Green River Formation (Utah, USA; Anderson and Dean, 1988). Long-term geomorphologic stability under seasonal climate provides favorable conditions for preserving varved structures at Clarkia (Zolitschka et al., 2015). The calculation of varve-years in the age model for the Site P-33 were solely based on grain-size variation ratios (K/Ti and Rb/Zr) because as the lakes shallowed, forming a *Konzentrat-Lagerstätte,* there was a detachment between fossil preservation (color* and Inc/Coh) and the varve formation.

APPENDIX B

SUPPLEMENTAL FIGURES

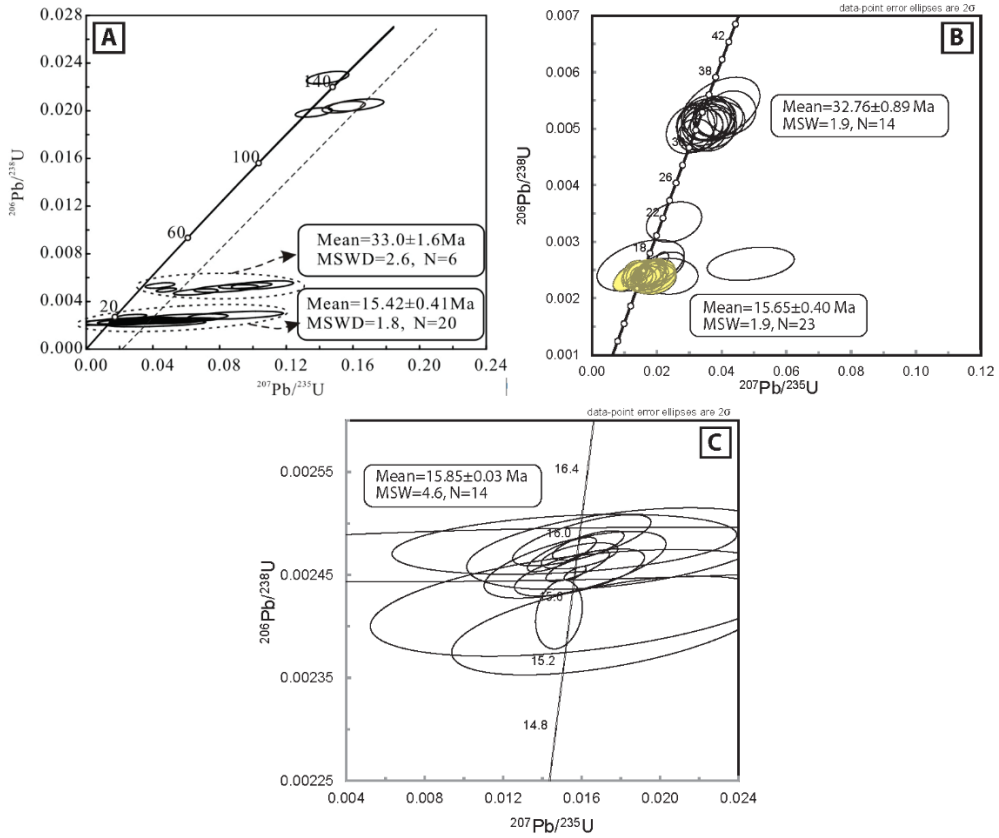

Figure B1 - Concordia diagrams of the volcanic ash layers units 4 and 5B. A) LA-ICP-MS analysis of Unit 4 sample (at China University of Geosciences at Wuhan). Two populations are found, in which the zircon grains yielded weighted mean $^{206}Pb/^{238}U$ ages of 33.0 ± 1.6 and 15.42 ± 0.41 Ma (MSWD = 2.6 and 1.8, respectively). B) LA-ICP-MS analysis of Unit 5B sample (at Texas A&M University). Two populations of zircon grains yielded weighted mean $^{206}Pb/^{238}U$ ages of 32.76 ± 0.89 and 15.65 ± 0.40 Ma (MSWD = 1.9). The highlighted subset of zircon grains was later analyzed via CA-ID-TIMS. C) CA-ID-TIMS analysis of the Miocene population from the Unit 5B sample (15.85 ± 0.03 Ma; MSWD = 4.6) previously analyzed by LA-ICP-MS (at Texas A&M University). The weighted mean $^{206}Pb/^{238}U$ ages is 15.78 ± 0.035/0.035/0.039 (uncertainties listed in order of analytical / including tracer / including decay constants). All zircon analyses from sample 2C are significantly older than the depositional age and are interpreted to be either detrital or xenocrystic grains. Reprinted from Höfig *et al.* (2021).

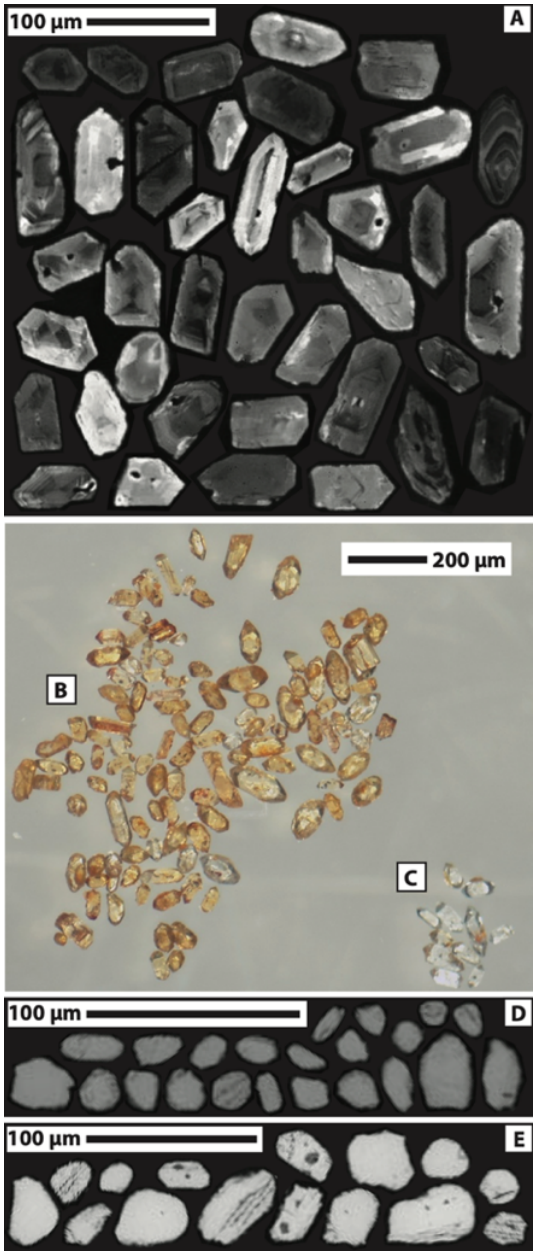

Figure B2 - Selected images of zircon grains found in the ash layers of Site P-33. A) Cathodoluminescence images of Miocene and Oligocene zircon grains of Unit 4 sample (dated via LA-ICP-MS; China University of Geosciences at Wuhan). B) Oligocene zircon population of Unit 5B (dated via LA-ICP-MS; Texas A&M University). C) Miocene zircon population of Unit 5B (dated via LA-ICP-MS and ID-TIMS; Texas A&M University). D) Detrital zircon grains of Unit 2C (dated via LA-ICP-MS; University of Arizona). E) Detrital zircon grains of Unit 4 (dated via LA-ICP-MS; University of Arizona). Reprinted from Höfig *et al.* (2021).

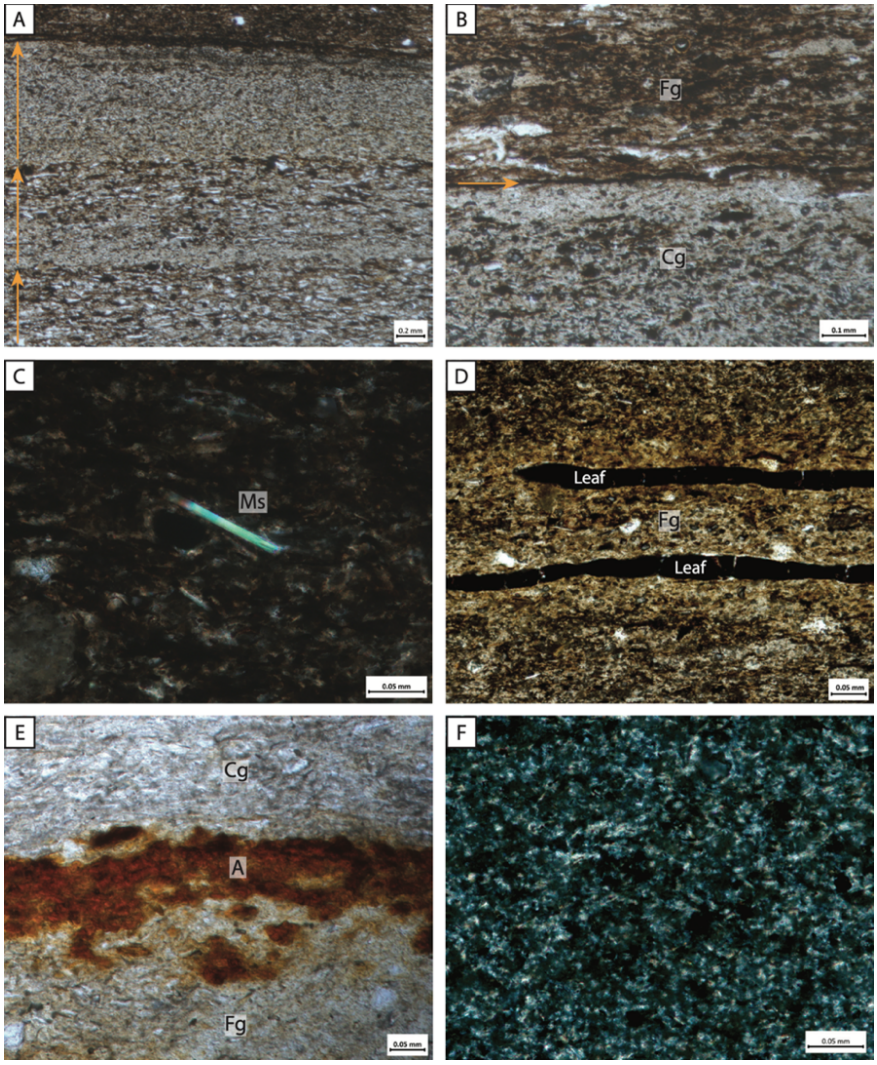

Figure B3 - Selected microphotographs of textural and mineralogical features found in the units of Site P-33. A) Varve couplets formed by fining-up cycles, which are represented by arrows in the image (plane-polarized light [PPL]). B) Contact between the dark, fine-grained layer (Fg) and light, coarse-grained layer (Cg). These layers vary in grain-size and proportions of detrital quartz, mica, opaque minerals, epidote, zircon, and apatite (PPL). C) Detrital muscovite (Ms) grain is a common occurrence in the varved-sediments of the unoxidized zone (cross-polarized light [XPL]). D) Fossil leaves (Leaf) distributed in the dark, fine-grained layer (Fg) (PPL). E) Iron-alteration product (A) percolating the contact between the dark, fine-grained layer (Fg) and light, coarse-grained layer (Cg) in the Unit 5A. This unit contains quartz, mica, and opaque minerals percolated with iron alteration products. (PPL). F) At Site P-33 the ashfall layers present ultra-fine-grain size. The matrix is formed by glass shards, quartz, and muscovite and rare accessory phases (cross-polarized light [XPL]). Reprinted from Höfig *et al.* (2021).

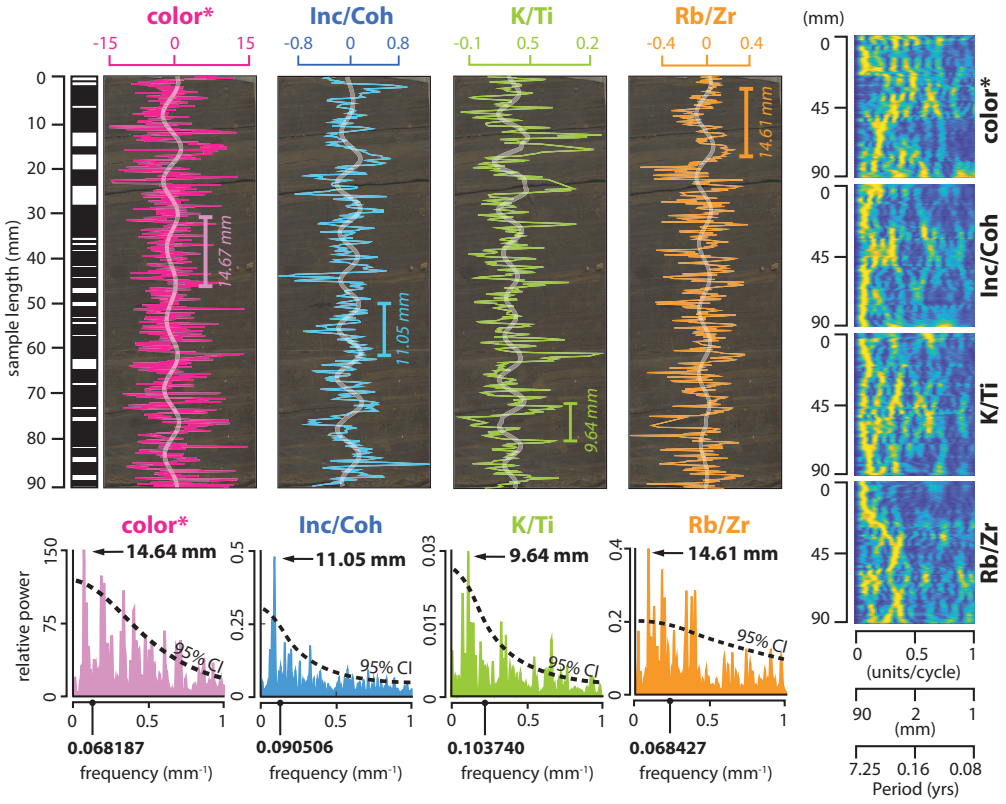

Figure B4 - Spectral analysis of Unit 2D. Frequency analysis of red-color intensity transect across the varves (color*), incoherent and coherent scatter (Inc/Coh), K/Ti and Zr/Rb ratios show depositional cycles at every 9.64-14.64 mm in Unit 2D. For the age model, the average between the values of four depositional cycles was used to decrease the scatter (9.64-14.64 mm). Signals of depositional cycles stand out above the 95% confidence interval in the power spectra and the Fast Fourier Transform processing (light-colored bands). Reprinted from Höfig *et al.* (2021).

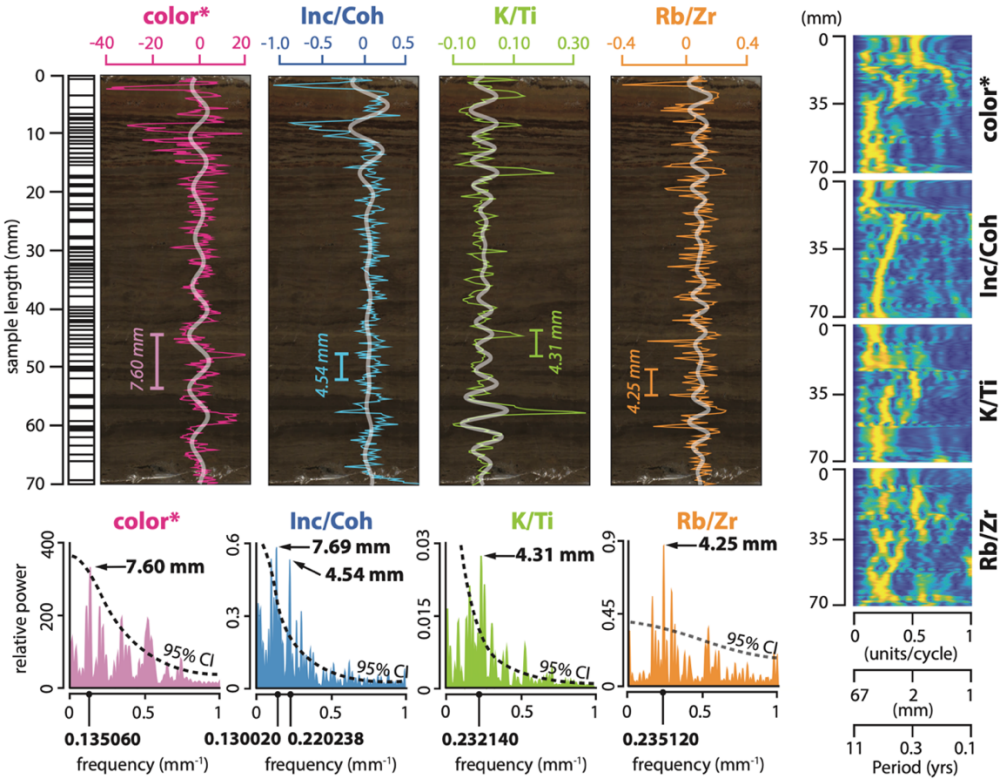

Figure B5 - Spectral analysis of the Unit 5A. Frequency analysis of red-color intensity transect across the varves (color*), incoherent and coherent scatter (Inc/Coh), K/Ti and Zr/Rb ratios show depositional cycles at every 4.25-7.69 mm in Unit 5A. The cyclicity of the *color data (7.60 mm) large deviates from the other indices, probably because it is less sensitive to sediment cycles in this oxidized unit with low organic carbon content. Consequently, for the age model, the average between three depositional cycle values based on Inc/Coh, K/Ti and Zr/Rb was used to decrease the scatter (4.25-4.54 mm). Signals of depositional cycles stand out above the 95% confidence interval in the power spectra and the Fast Fourier Transform processing (light-colored bands). Reprinted from Höfig *et al.* (2021).